Engineering Fracture Mechanics 271 (2022) 108619

Contents lists available at ScienceDirect

Engineering Fracture Mechanics

journal homepage: www.elsevier.com/locate/engfracmech

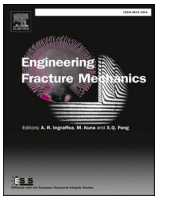

# Analysis of mode I fracture toughness of adhesively bonded joints by a low friction roller wedge driven quasi-static test

E. Meulman [a,*], J. Renart [a], L. Carreras [a], J. Zurbitu [b]

[a] AMADE, Polytechnic School, University of Girona, Campus Montilivi, s/n, 17071 Girona, Spain
[b] Ikerlan Technology Research Centre, Basque Research and Technology Alliance (BRTA), Arrasate-Mondragón, Spain

ARTICLE INFO

*Keywords:*
Wedge driven test
Fracture energy
Mode I
Bonded joint

ABSTRACT

In structural bonded joint design, mode I fracture toughness is a key mechanical property. Using a sliding wedge driven test to measure the fracture toughness of an adhesive is a good alternative to the standardised DCB test. However, with a sliding wedge driven test, the friction between the wedge and the specimen is difficult to determine and has an influence on the fracture toughness data reduction. In this work, we present a relatively small and simple mode I fracture toughness test setup with a roller wedge, which can potentially be used without a test machine to make a quick and affordable approximation of the mode I fracture toughness. DCB test results of the specimens are used as a reference to compare the roller wedge driven test method against. Results show that the friction of the roller wedge is significantly lower than a sliding wedge, and thanks to the low friction of the rollers the required driving force of the wedge is likewise low. Therefore, a human hand can apply a high enough force to the wedge by rotating a threaded bar to push down the wedge. Controlling the displacement rate by rotating a threaded bar by hand is difficult, therefore this method appears to be only suitable for non-rate sensitive adhesives. By comparing the roller wedge force and J-integral data reduction method, it has been shown the roller wedge force data reduction method is less sensitive to measurement errors. The proposed Roller Wedge Driven test method could potentially be an alternative mode I fracture toughness test method for bonded joints.

## 1. Introduction

Structural adhesive bonds are increasingly used in industry as an alternative to mechanical joints [1]. One of the advantages of structural adhesive bonds is that the need for more traditional fasteners becomes obsolete, consequently making the structure lighter, smoother and distributing stresses over a larger area (i.e., stress concentrations are limited). Nevertheless, there are some disadvantages to using adhesives for structural bonding such as limited capacity for visual inspection, high quality surface preparation being required, controlling process parameters being important and adhesives are environmentally sensitive. Material characterisation of an adhesive is essential to design a structural bond for its service load cases.

When designing a bonded joint, one of the key adhesive mechanical properties is fracture toughness. A bonded joint is usually loaded with a mixed mode which is a combination of mode I and II [1]. Pure mode I and II fracture toughness test results show that, in

* Corresponding author.
*E-mail addresses:* edwin.meulman@udg.edu (E. Meulman), jordi.renart@udg.edu (J. Renart), laura.carreras@udg.edu (L. Carreras), jzurbitu@ikerlan.es (J. Zurbitu).

https://doi.org/10.1016/j.engfracmech.2022.108619
Received 15 February 2022; Received in revised form 19 May 2022; Accepted 10 June 2022
Available online 14 June 2022

**Nomenclature**

| | |
|---|---|
| $a$ | crack length |
| $a_c$ | corrected crack length |
| $a_e$ | crack length with exact contact point |
| $B$ | width of specimen |
| $C$ | compliance |
| $d_{ini}$ | initial wedge displacement for fracture toughness calculation |
| $d_{lim}$ | wedge displacement limit |
| $E_x$ | longitudinal Younǵs modulus |
| $E_f$ | back-calculated modulus of the substrate |
| $\Delta$ | correction by taking the intercept of $C^{1/3}$ against $a$ |
| $D_w$ | diameter of the wedge |
| $E_y$ | transversal Younǵs modulus |
| $F_{push}$ | force to push the wedge |
| $F_{Push\|s}$ | force to push the wedge simplified data reduction method |
| $G$ | energy release rate |
| $G_c$ | critical energy release rate |
| $G_e$ | energy release rate with exact contact point |
| $G_{xy}$ | in-plane shear modulus |
| $h$ | thickness of the adherend |
| $J$ | energy release rate with J-integral method |
| $N$ | correction to compensate for the stiffness of the DCB bonding blocks |
| $P$ | opening force |
| $t_a$ | bondline thickness |
| $r_w$ | radius of the wedge |
| $\delta_y$ | opening displacement |
| $\theta$ | adherend tip rotation angle |
| $\theta_c$ | adherend tip rotation angle at critical energy release rate |
| $\theta_{ini}$ | adherend initial rotation angle |
| μ | friction coefficient |
| $\chi$ | crack length correction factor |
| CBBM | Compliance Based Beam Method |
| CBT | Corrected Beam Theory |
| COF | Coefficient of Friction |
| DCB | Double Cantilever Beam |
| LVDT | Linear Variable Displacement Transducer |
| RWD | Roller Wedge Driven |
| WDT | Wedge Driven Test |
| WDT+ | Wedge Driven Test simplified data reduction method |

general, fracture toughness in mode I is lower than in mode II [2]. To measure pure mode I fracture toughness, the bonded joint is cleaved or peeled. This can be done with different test methods, the most common of which are standardised test methods based on the double cantilever beam test (DCB) and are described in ASTM D5528-01 [3] and ISO-25217 [4]. The beams can be separated by load control, something which is rarely done, or by a constant opening displacement rate [5]. With a constant opening displacement rate of the beams, the crack growth rate (crack growth over time) will not be constant during the test. On the other hand, applying a constant load will very likely result in unstable crack propagation.

The data reduction method described in ISO-25217 [4] is based on corrected beam theory (CBT). For the CBT data reduction method, the measurement of crack length is required, which is preferably avoided since this could introduce significant errors as a result of the non-objective visual method that is generally used for crack length measurement [6]. Alternative data reduction methods that do not require crack length measurements are the compliance based beam method (CBBM) [7] and the J-integral method [8]. For the CBBM method, the flexural modulus of the specimen needs to be obtained. Therefore, testing specimens with different materials means the CBBM method is labour intensive. The J-integral method, however, only depends on rotation measurements of the adherend tip and the applied load.

Another method to cleave a bonded joint is by using a wedge. The same type of specimen as in the DCB test is used but in this case a wedge is introduced in between the two adherends (beams) until crack propagation starts. Then the wedge is retained in its position and over time the crack will continue to propagate. ASTM D-3762 [9,10–12], also known as the Boeing wedge test, used to be the standard wedge test method. However, in July 2019 the standard was withdrawn because it had not been updated for the last eight

years. The wedge test was never originally designed to be used for a quantitative measurement of mode I fracture toughness but instead was meant to be used as a qualitative test to determine if an adhesive properly bonds to an adherend. Authors like Cognard et al. [13] and Plausinis et al. [14] have tried to use the Boeing wedge test to obtain quantitative properties for bonded joints. Variations on the wedge test are designed like, for example, the wedge driven test (WDT) [6,15–17]. A significant advantage of the wedge driven test is that it can be assumed that the crack length during propagation is on average constant. In this case, the crack length is defined as the distance between the crack tip and the tip of the wedge. As a result, crack measurement is objective since during the crack propagation phase (only the case for stable crack propagation) the incremental displacement of the wedge, provided by the test setup crosshead, equals the crack length increase. This principle could also be used for creep or durability testing where a constant load is applied to the wedge, which then moves, under stables crack propagation, at the same rate as the crack tip. This means for a certain load a constant crack growth rate could be obtained over the complete crack length. Unlike the Boing wedge test, where the crack growth rate slows down when the crack is propagating, because the wedge is stationary.

To determine the fracture energy with a test, the total energy that goes into the system and how much of this energy is used for creating the crack surfaces (energy release rate, $G$) needs to be known. The critical energy release rate ($G_c$) is a material property and indicates the resistance to crack growth. In other words, if $G \geq G_c$ crack growth occurs in the material [18]. Considering a WDT, the wedge is in direct contact with the adherends and slides along them creating friction. The energy that is required to overcome the friction force is difficult to measure directly. Therefore, determining the fracture toughness based on the total amount of energy put into the system is not evident unless the friction force can be eliminated. Different authors have shown that, even when using low friction materials, the sliding friction forces cannot be neglected when determining fracture toughness [19,20]. Likewise, it is also not evident to determine the friction coefficient as a single value since the friction coefficient is not constant during the test [6]. Glessner et al. [21] proposed a WDT design that uses a roller wedge to separate the adherends and reduce friction force to a minimum. Potentially the rollers result in a low enough friction force that the friction force can be neglected. However, the authors did not present

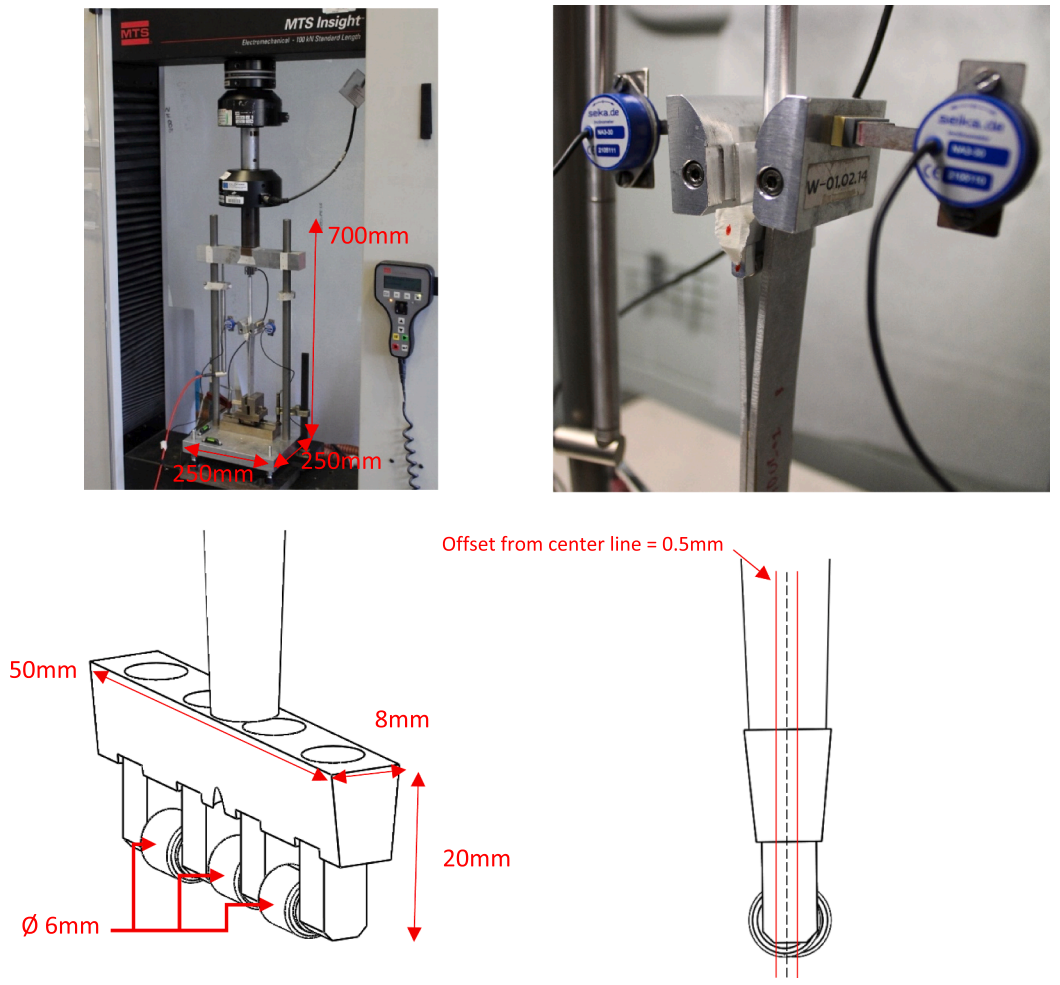


**Fig. 1.** Top left: RWD test setup. Top right: Roller wedge inserted in specimen. Bottom left: Sketch of roller wedge design with three rollers. Bottom right: Side view sketch of wedge where the middle roller and the two outer rollers have an offset of 0.5 mm (solid red line) from the wedge centre line (black dashed line).

the friction force of the roller wedge compared to a different method to show that the friction force can indeed be neglected when using a roller wedge. Adams et al. [22] designed the 'Smart Wedge' concept which also uses rollers to separate the adherends. The rollers are directly connected to a load cell, therefore the specimen opening load can be directly measured. With the 'Smart Wedge' concept, crack measurement is not required to be estimated during the test, however, flexural rigidity of the adherends does need to be measured to be able to calculate the crack length when post-processing the test results.

For the WDT, Renart et al. [20] developed a data reduction method to determine fracture toughness. The data reduction method requires the measured load to drive the wedge into the specimen and takes the friction coefficient into account. Manterola et al. [6] simplified the WDT data reduction method by making use of inclinometers to measure the rotation of the adherend tips and, as a result, obtain the fracture toughness of the bonded joint. This simplified method avoids a coefficient of friction (COF) estimation and the bondline thickness is taken into account. The proposed simplified data reduction method (WDT + ) has shown to be less sensitive to displacement rate, bondline thickness, wedge thickness and type of adhesive.

All the Mode I fracture toughness test methods found in literature require a test machine to perform the experimental test. For quality control, the DCB is the accepted standardized test method in industry. For instance, for preliminary design purposes like material selection, it could be desired to test some different material combinations to obtain a fracture toughness approximation. The DCB test, which requires a test machine, can be time consuming and costly to perform. It would be beneficial to have a test method that can measure the mode I fracture toughness of a bonded joint in a faster and simpler way. In this work, we present the Roller Wedge Driven (RWD) test setup design which, when compared to the other methods described in this introduction, is a simpler test method. The RWD test setup is based on a concept design from Glessner et al. [21] and a patent of the Ikerlan Technology Research Centre and AMADE [23]. The latter proposes a roller wedge with a data reduction method that is based on adherend rotation measurement with inclinometers. Measuring directly the wedge driving force to obtain fracture toughness properties is likely a better option. This is also what Glessner et al. did by assuming that the friction of the roller wedge is zero. However, no comparison was made with other methods to confirm the friction can indeed be assumed zero. The authors of this work believe this deserves further investigation.

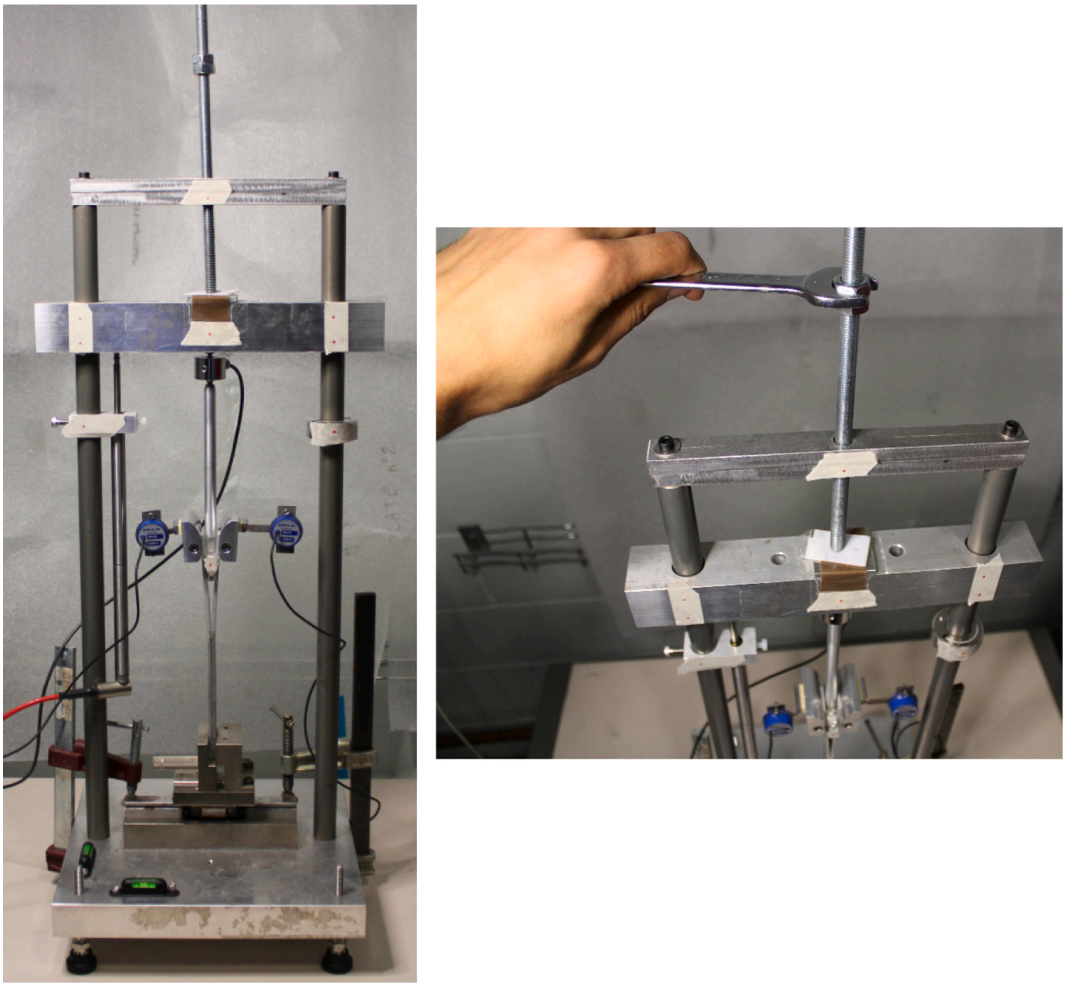

**Fig. 2.** RWD manual test setup configuration with a threaded bar that pushes the loading beam of the wedge down when rotated with a spanner.

In theory, one could apply the manual load by just pressing the wedge into the specimen by hand, however this will probably result in unstable crack growth since applying the force by pushing by hand is difficult to control. A manual mechanism is required to apply a more control displacement to the wedge. As a result making it a quick and easy-to-perform test that can assess many specimens in a relatively short timeframe.

In section 2, the authors present the RWD test method and setup, as well as the experimental testing campaign carried out in two different laboratories. The comparison between the DCB and RWD test results are presented in section 3 and the results obtained are discussed in section 4. Finally, section 5 describes the conclusions of this work.

## 2. Methodology

### 2.1. The roller wedge driven test (RWD)

The RWD test setup (Fig. 1, top left) has a wedge that consists of three rollers (Fig. 1, bottom left). A clamp and a linear carriage system hold the specimen in a vertical position in line with the roller wedge. A bearing connects the roller wedge with the horizontal loading beam. The bearing makes it possible that the roller wedge can rotate around its longitudinal axis making sure all rollers make contact with the adherends and preventing potential mode III loading of the specimen. An aluminium block is mechanically attached to each end of the adherend. These aluminium blocks (Fig. 1, top right) open the ends of the adherends when the roller wedge is pushed against the aluminium blocks. This makes it possible to smoothly enter the round rollers of the wedge in between the narrow gap between the adherends [20].

An HBM WA-T-50 linear variable displacement transducer (LVDT) with a precision of 0.2% measures the displacement of the roller wedge. The LVDT attaches to one of the vertical guiding columns and is in contact with the horizontal support beam of the roller wedge. The support rod of the roller wedge contains a load cell (HBM U9C-500) with a precision of 0.2% to be able to measure the applied force that drives the roller wedge into the specimen. An inclinometer (NA3-30 from SEIKA Mikrosystemtechnik GmbH) with a precision of 0.005° is attached to each of the aluminium blocks at the opening end of the adherends to be able to measure the rotation angle of the adherend tips (Fig. 1 top right). As explained in section 1, the inclinometers are only required for the J-integral data reduction methods and therefore used as a reference measurement. We use an MTS Insight 100 kN for the RWD quasi-static mode I fracture tests. The RWD quasi-static tests are performed with displacement control. All displacement data in this research are measured with the LVDT. Additionally, it is possible to run the test manually (by hand) by moving the RWD test setup loading beam with a threaded bar and a support allocated on top of the two guiding columns (Fig. 2).

The calculation of the energy release rate applied to the specimen is based on the WDT data reduction method [20] and reads:

$$G = \frac{3}{4}\frac{E_x h^3 \delta_y^2}{a_c^4} \tag{1}$$

where $E_x$ is the longitudinal Youngs modulus of the adherend, $h$ is the thickness of the adherend, $a_c$ is the corrected crack length and $\delta_y$ is the opening displacement at the contact point between the roller and the adherend. It is assumed that the roller wedge rollers are small enough in diameter that the simplified contact point principle can be applied [20] and additionally taking into account the bondline thickness ($t_a$) and the diameter of the wedge ($D_w$) [6]:

$$\delta_y = \frac{D_w - t_a}{2} \tag{2}$$

The corrected crack length ($a_c$) in the data reduction method (1) takes into account the flexibility of the adherends and corrects the crack length ($a$) with the following equation:

$$a_c = a + \chi h \tag{3}$$

Parameter $\chi$ is the crack length correction factor [24]:

$$\chi = \sqrt{\frac{E_x}{11G_{xy}}\left[3 - 2\left(\frac{1.18\frac{\sqrt{E_x E_y}}{G_{xy}}}{1.18\frac{\sqrt{E_x E_y}}{G_{xy}} + 1}\right)^2\right]} \tag{4}$$

where $E_x$ and $E_y$ are the Youngs modulus in the longitudinal and transversal direction, respectively and $G_{xy}$ is the in-plane shear modulus. The crack length correction factor is added to crack length $a$ after multiplication by $h$, which is the thickness of the adherend. The crack length correction factor compensates for the rotation of the adherends near the crack tip, since the elastic beam theory does not take this rotation into account and therefore underestimates the crack length.

Since the simplified contact point between the rollers and the adherends is assumed, the simplified data reduction method can also be used [20]:

$$F_{Push|s} = \frac{E_x B h^3 r_w \left(\frac{3r_w}{2a} + \mu\right)}{2a^3\left(1 - \frac{3r_w}{2a}\mu\right)} \tag{5}$$

In which $F_{Push|s}$ (the applied force) is measured with the load cell, $B$ is the width of the specimen, $h$ is the thickness of the adherend and $r_w$ is the wedge tip radius (i.e., the roller radius). The friction coefficient μ is assumed to be negligible and therefore taken as zero [21]. After performing the test, $F_{Push|s}$ is known from the test results. This means only one unknown variable remains: $a$. Numerically solving $a$ in equation (5) and substituting that value in equation (3) will provide parameter $a_c$. The value of $a_c$ can be used to determine $G$ with equation (1). By combining equations (1) to (5), the RWD force equation is obtained:

$$G = \frac{3}{4}\frac{E_x h^3 \delta_y^2}{\left(\sqrt[4]{\frac{3}{4}\frac{E_x B h^3 r_w{}^2}{F_{Push|s}}} + \chi h\right)^4} \tag{6}$$

The principle of the J-integral method used for the DCB test can also be used for the RWD test if inclinometers are used and is based on [6]:

$$J = 2\frac{P}{B}\tan\theta \tag{7}$$

where $B$ is the specimen width, $P$ the adherend opening force and $\theta$ is the adherend tip rotation angle. In the DCB test the adherend opening force $P$ can directly be measured with the load cell, whereas with a wedge test a conversion needs to be performed to obtain the adherend opening force P from the measured driving force of the wedge [6]:

$$P = \frac{E_x B h^3 \delta_y}{4a^3} \tag{8}$$

In case of the simplified contact point between the roller and the adherend, $\delta_y$ can be determined with equation (2). The crack length $a$ can be estimated based on the opening displacement and the adherend tip rotation angle [6]:

$$a = \frac{3}{2}\frac{\delta_y}{\tan\theta} \tag{9}$$

Equations (7) to (9) can be combined into a single equation, RWD J-integral:

$$J = \frac{4}{27}\frac{E_x h^3 \tan^4\theta}{\delta_y^2} \tag{10}$$

The J-integral method as described is a useful method to be able to compare obtained energy release rates and fracture toughness from the different test methods used for this experimental campaign.

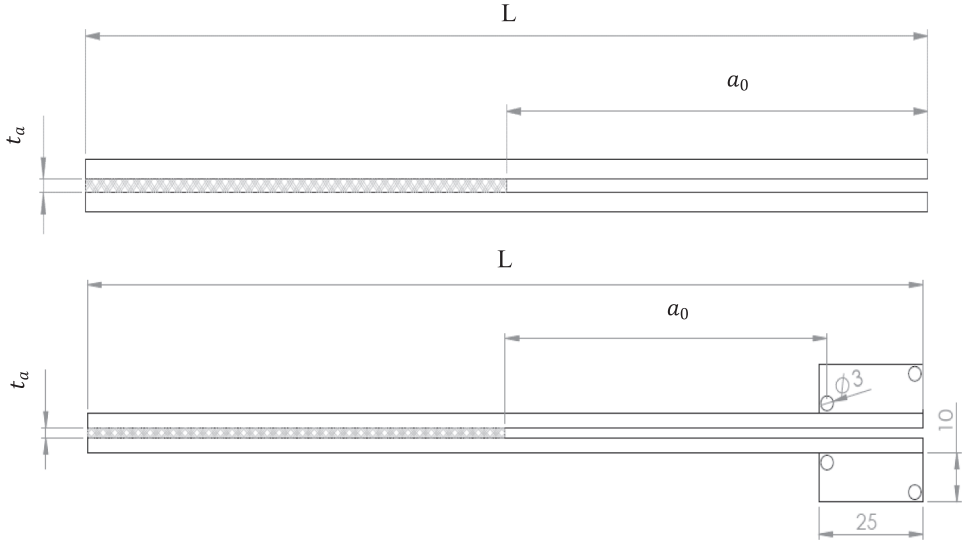


**Fig. 3.** Specimen geometry, top: for RWD test, bottom: for DCB test including two blocks with holes to attach the specimen to the test machine. Only the two holes in the block closest to the adherends are used to make the block function as a hinge. The second hole is only there so the blocks can be re-used for another DCB test.

### 2.2. DCB tests

The DCB tests were performed according to the DCB test standard [4]. Both the CBT and DCB J-integral based data reduction methods were applied to the results to obtain the mode I fracture toughness of the specimens. For the CBT method, the crack length needs to be measured. We measured the crack length visually with a camera (Canon 550D and macro lens EF100). By marking the side of the specimen, it is possible to determine what the crack length is at any moment during the test. The DCB J-integral method makes use of the rotation of the adherends and the applied opening load during the test. The inclinometers measured the rotation angle of the adherends and are the same inclinometers as used for the roller wedge driven test. The equation for the DCB J-integral is [6,25]:

$$J = \frac{P}{B}\theta_{rel} \tag{11}$$

The load that is measured to open the DCB specimen is $P$, the width of the specimen is $B$ and $\theta_{rel}$ is the relative rotation between the adherends.

### 2.3. Experimental testing campaign

We manufactured the specimens in the AMADE research group laboratory. Two 200 mm long, 25 mm wide and 3 mm thick aluminium Al 7075-T6 adherends were bonded with a rigid structural adhesive. The bondline thickness $t_a$ was between 0.4 and 0.6 mm (Fig. 3). The rigid adhesive is a methacrylate-based Araldite 2021–1. Araldite 2021–1 has a glass transition temperature of 80 °C. The aluminium adherend has a Young's modulus of 71 GPa, shear modulus of 27GPa and a yield strength of 550 MPa [6,26].

We pre-treated the adherends by sanding them with sandpaper P80, degreasing them with acetone and, just before bonding, cleaning them with high grade alcohol. The adhesive was cured in an oven set at 60 °C for 16 h. Teflon spacers ensured a constant bondline thickness of the specimen during its manufacture. The Teflon spacers were removed once the curing process had been completed. The initial crack length ($a_0$) was 100 mm for the RWD specimens and 37 mm for the DCB specimens. The DCB standard [4] states that the DCB specimens should be painted white and marked on one side to be able to visually measure the crack length during a test. Metal blocks with holes bonded to the DCB specimen made it possible to attach the specimens to the testing machine.

We performed all the RWD tests in this research in the ISO17025 and NADCAP certified AMADE research group testing laboratory at the University of Girona, testing at an ambient temperature ($23^{\circ}\pm2^{\circ}C$, 50 ±5 % RH). A total of five specimens were tested with the DCB test method: three specimens at the AMADE laboratory (DCB_01 to DCB_03) and two at the IKERLAN Technology Research Centre (DCB_04 & DCB_05). The test machine applied an opening displacement rate of 2 mm/min to the DCB specimens. Four specimens were tested with the RWD test setup (RWD_01 to RWD_04) at a wedge displacement rate of 5 mm/min. Additionally three specimens (RWD-M_01 to RWD-M_03) were tested with the RWD test setup without using the test machine, but by manually applying a load to the wedge (as described in section 2.1). Table 1 shows an overview of the tested specimens.

## 3. Results

This section describes the results from the three types of mode I fracture tests. First, we present the DCB test results, followed by the results from the RWD test method using the RWD force data reduction method to determine the fracture toughness. Then, we describe the results from the RWD manually-loaded test method using the same RWD force data reduction method. This section also contains the results from the RWD J-integral data reduction method applied to both test methods. Finally, an overview of all the test methods and different data reduction methods is visually depicted using a bar plot.

### 3.1. DCB test

The force–displacement curves of the DCB specimens are plotted in Fig. 4. The initial stiffness of all five specimens is very similar. The peak force is for all specimens at a similar opening displacement.

The rotation angles measured at the adherend tips are used to determine the energy release rate with the DCB J-integral method [25] (Fig. 5). The first 5 to 10 mm of the opening displacement after the peak force shows some deviation between the different specimens in terms of energy release rate. Later during the test, the energy release rate of most specimens converges to range between 2.5 and 3.5 N/mm (considering the range between the peak force and 30 mm of opening displacement).

The CBT method is based on a visual discontinuous measurement of the crack length. All the data points related to the crack length

**Table 1**
Overview of tested specimens.

| Specimen | Test method | Disp. rate (mm/min) | Specimen thickness (mm) | $t_a$(mm) | No. of specimens |
|---|---|---|---|---|---|
| DCB_0x | DCB | 2 | 6.47 ± 0.04 | 0.47 ± 0.04 | 5 |
| RWD_0x | RWD | 5 | 6.46 ± 0.04 | 0.46 ± 0.04 | 4 |
| RWD-M_0x | RWD Manual | 38.2* | 6.48 ± 0.09 | 0.48 ± 0.09 | 3 |

* Could only be determined after the test and is the average measured displacement rate.

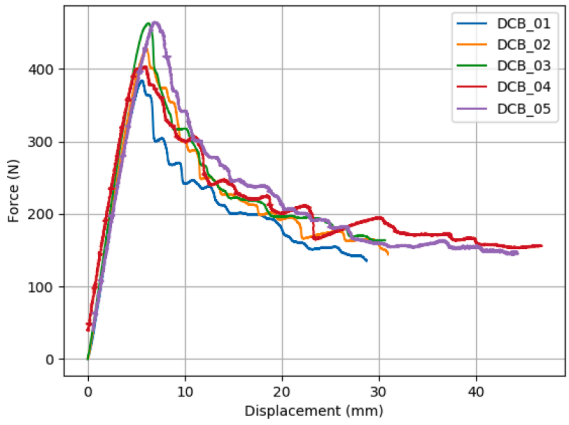


**Fig. 4.** Force-displacement curves of DCB specimens.

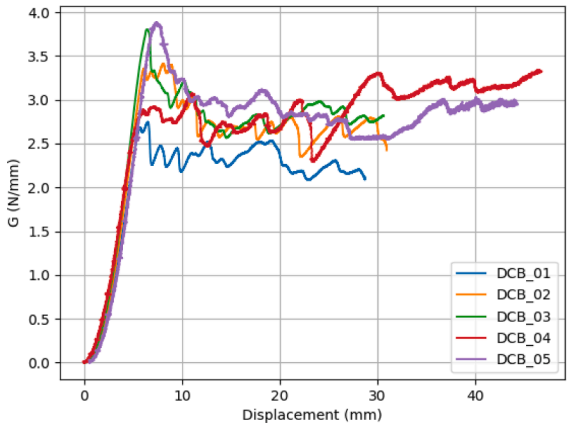


**Fig. 5.** Energy release rate vs. opening displacement of DCB specimens determined with the DCB J-integral method.

measurement are expressed in energy release rate and plotted against the opening displacement in Fig. 6. The same behaviour as the DCB J-integral method can be observed, where the energy release rate converges to a range between 2.5 and 3.5 N/mm.

In Fig. 7, both the results of the DCB J-integral and CBT method are plotted as comparison. The specimens on the left in Fig. 7 are those that were tested at the AMADE laboratory and those on the right were tested at the Ikerlan Technology Research Centre. Both methods show a good correlation as the difference between the two data reduction methods is less than 2% for the average energy release rate for all tested DCB specimens.

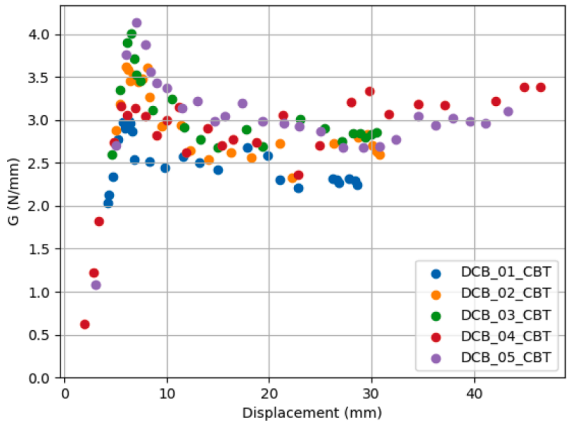


**Fig. 6.** Energy release rate vs. opening displacement of DCB specimens determined with the CBT method.

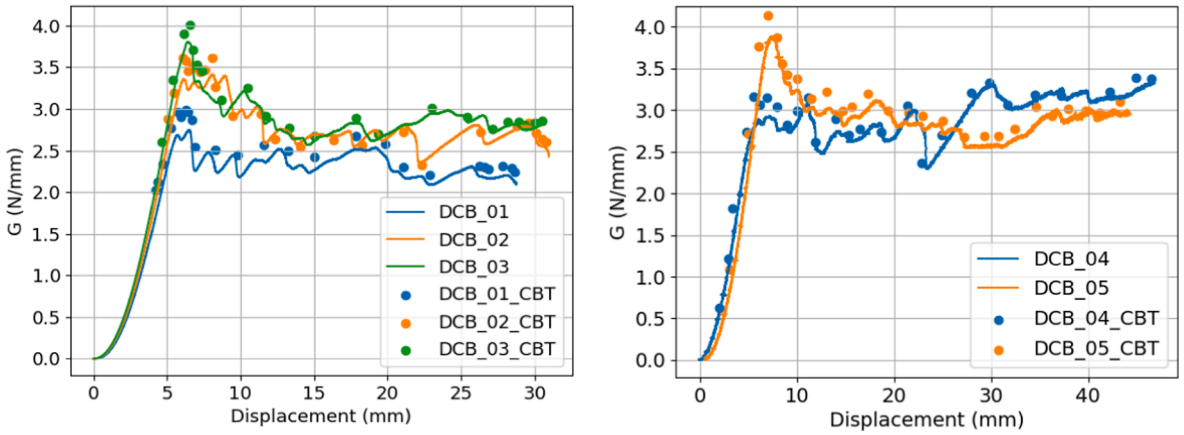


**Fig. 7.** Comparison of DCB J-integral and CBT method. Specimens on the left were tested at the AMADE laboratory and those on the right at the Ikerlan Technology Research Centre.

For all specimens we observed a cohesive failure of the adhesive like, for example, specimen DCB_03 shown in Fig. 8. To the right of the red line is the fracture surface created during the DCB test. The adhesive is a glassy polymer that forms voids during the fracture process as can be seen as small black dots in the DCB crack propagation section. To the left of the red line, the fracture surface was formed by opening the specimen using lab tools to be able to inspect the fracture surface of the specimen (this is not part of the test). It is observed that the fracture surface changes, this could indicate that this type of polymer is strain rate sensitive, however, the failure mode remains as cohesive failure.

Table 2 shows the average values obtained from the DCB tests. The average is taken from the peak force until the test was stopped. The average energy release rate of this range, where stable crack propagation take place, is considered as the fracture toughness of the specimen. There is some spread in the average values of the energy release rates for the different specimens. The average of all specimens is 2.719 N/mm with a standard deviation of 0.228 N/mm, and 2.772 N/mm with a standard deviation of 0.184 N/mm for the DCB J-integral and CBT method, respectively. The averages of both methods correlate well (difference less than 2%) and fall within standard deviation. The DCB test and the CBT data reduction method are standardised and widely accepted, therefore these results were used as a benchmark for the other test results presented in the following sections.

Table 2 shows a column indicated with $E_f$ which is the back-calculated modulus of the substrate [27] and is used to check the stiffness of the substrate against the expected modulus of 71000 N/mm$^2$. The equation for $E_f$ is [27]:

$$E_f = \frac{8(a+|\Delta|)^3}{(C/N)Bh^3} \tag{12}$$

Where $a$ is the crack length, $C$ is the compliance,$B$ specimen width, $h$ adherend thickness, $\Delta$ a correction by taking the intercept of $C^{1/3}$ against $a$ and $N$ a correction to compensate for the stiffness of the DCB bonding blocks. In Table 2 the standard deviations in the column are the standard deviations found for the result of one specimen (i.e. the average value from the propagation points). The

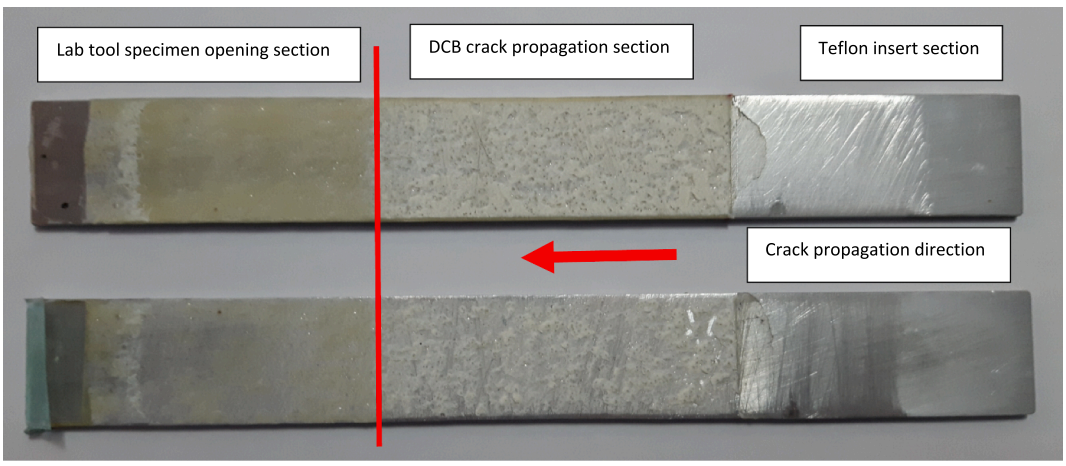


**Fig. 8.** Cohesive fracture surface of specimen DCB_03, to the right of the red line the adhesive fractured during the DCB test, to the left the specimen fractured during the process of splitting the adherends with lab tools to be able to inspect the fracture surface (later not part of the test).

**Table 2**
Overview of average DCB test results. The standard deviations in the column are the standard deviations found for the result of one specimen. The standard deviation in the last row is the standard deviation found when taking the average value for all specimens tested.

| Specimen | $G_c$- J-int (N/mm) | | $G_c$– CBT (N/mm) | | $E_f$(N/mm$^2$) | |
|---|---|---|---|---|---|---|
| | Avg. | Std. Dev. | Avg. | Std. Dev. | Avg. | Std. Dev. |
| DCB_01 | 2.299 | 0.127 | 2.461 | 0.133 | 61120* | 1397 |
| DCB_02 | 2.676 | 0.125 | 2.662 | 0.189 | 77,685 | 2123 |
| DCB_03 | 2.811 | 0.130 | 2.915 | 0.177 | 69,586 | 574 |
| DCB_04 | 2.951 | 0.256 | 2.888 | 0.252 | 72,323 | 1943 |
| DCB_05 | 2.856 | 0.154 | 2.933 | 0.181 | 73,113 | 1234 |
| Average: | 2.719 | | 2.772 | | 70,765 | |
| Std. Dev. | 0.228 | | 0.184 | | 5482 | |

* The back-calculated modulus deviates more than 10% from the expected modulus (71000 N/mm$^2$) and therefore the fracture toughness results of this specimen should be considered suspect [27].

standard deviation in the last row is the standard deviation found when taking the average value for all specimens tested.

### 3.2. Roller wedge driven test

The force–displacement curves of the RWD specimens are plotted in Fig. 9 (left y-axis). The initial stiffness of the specimens is very similar for the four specimens tested with the RWD test setup. This is followed by a peak force where, once the force drops, moves into a more stable region. Specimen RWD_01 shows a high rise in force - around 40 mm of wedge displacement (dotted line), indicating an increase in resistance that is likely caused by an external influence. After testing, none of the adherends showed any permanent deformation. Likely, the resistance changed due to local adherend surface change. In Fig. 8 a thin layer of adhesive is visible on the non-bonded adherend surface where there is the transition from bonded to non-bonded area. There was a Teflon spacer placed to during manufacturing to create the adhesively bonded and non-bonded area. Adhesive flowed underneath the Teflon spacer during the specimen manufacturing process when the adherends were pressed together. This part of the specimen is neglected for the fracture toughness calculation and in the following plots.

The RWD force data reduction method (equation (6)) is applied to determine the energy release rate of the RWD specimens that are plotted in Fig. 9 (right y-axis). Since the RWD force data reduction method only uses the measured force from the test results as the input value, the plot is similar to the force–displacement plot and, therefore, both can be plotted using two y-axes (Fig. 9). To determine the average fracture toughness of the specimens, the same cut-off criteria as for the DCB J-integral method is used, i.e., after the crack has initiated. Fig. 10 shows an example of the measured rotation angles where a dashed line named $d_{ini}$ indicates the initial wedge displacement where it is assumed that the crack propagation phase already has initiated. The dashed line of $d_{lim}$ cuts out the spikes in the results caused by the roller wedge being in contact with the adhesive. The section between $d_{ini}$ and $d_{lim}$ can be plotted as a resistance curve (R-curve), as shown in Fig. 11. The average energy release rate of the R-curve is considered as the fracture toughness of the specimen. About 25 mm is the maximum crack extension that can be measured with these type of specimen before the roller wedge meets the adhesive, which then influences the measured results by increasing the resistance to the wedge. It seems that, besides the fluctuations in the R-curve of the different specimens, all converge to an energy release rate of about 3 N/mm.

It must be noted that the average rotation angle as is, for example, plotted in Fig. 10, is not directly used in the RWD J-integral reduction method. After manufacturing the specimens it was noticed that, besides using Teflon spacers to ensure a constant bondline thickness, the adhesive shrinks slightly during the curing the process. This results in the adherends not being completely parallel and showing a minimal V like shape. This initial rotation, $\theta_{ini}$, of the adherends is calculated based on specimen dimensions and is added as

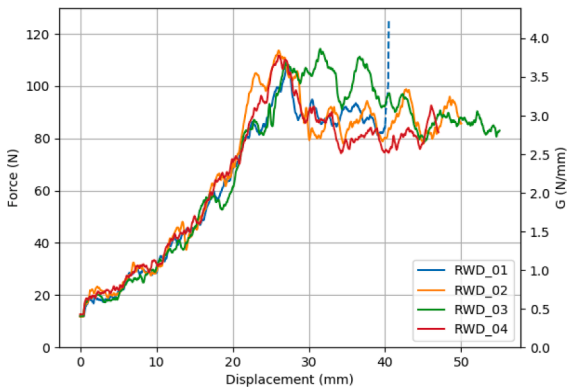


**Fig. 9.** Force-displacement and G-displacement curves of RWD specimens.

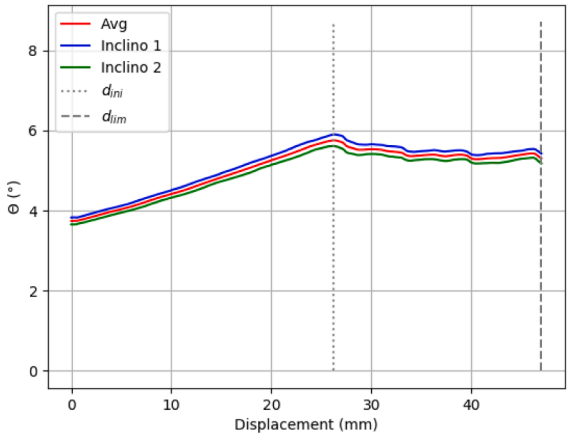


**Fig. 10.** Specimen RWD_04 as an example of how the $d_{ini}$ and $d_{lim}$ cut-offs determine the range over which the average energy release rate is calculated and is considered as the fracture toughness of the specimen.

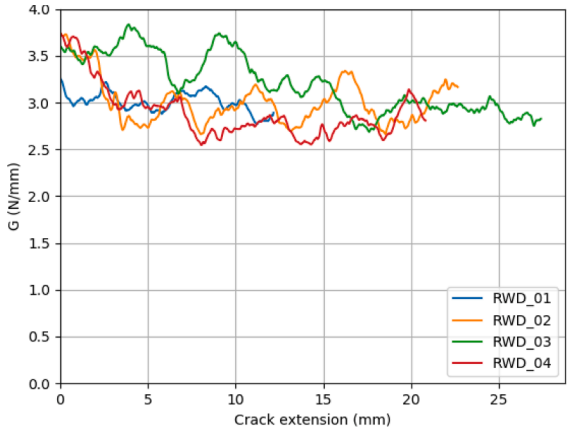


**Fig. 11.** Resistance curves (R-curves) of RWD specimens.

a correction factor to the average measured rotation angle. At the bonded section of the specimen, 30 mm and 90 mm from the short side of the specimen, a thickness measurement is taken using a micrometre. Over this distance the difference in thickness is used to calculate the initial angle ($\theta_{ini}$) of the adherends relative to each other. The average value for $\theta_{ini}$ found for all RWD specimens is 0.042°.

In Fig. 12, the results obtained with the RWD J-integral data reduction method are plotted. The same initial peak is observed after

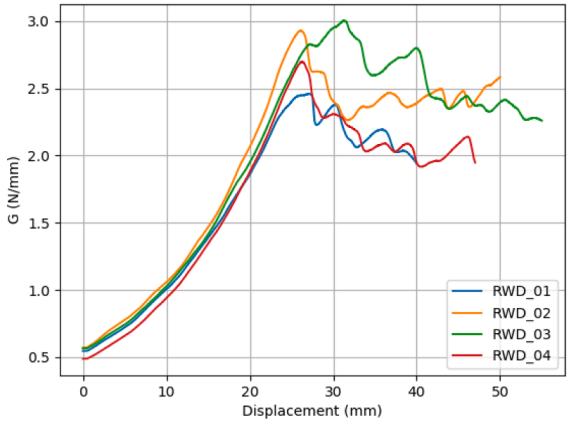


**Fig. 12.** Energy release rate vs. roller wedge displacement of RWD specimens determined with the RWD J-integral data reduction method.

which the energy release rate drops to a more stable value. The fluctuations with the inclinometers are less severe compared to using the measured force to determine the energy release rate. Using the RWD J-integral data reduction method, the energy release rate converges for specimens RWD_02 and RWD_03 to 2.4 N/mm, while specimens RWD_01 and RWD_04 are lower and converge to 2.0 N/mm.

For all the specimens, the cohesive failure of the adhesive is observed as being similar to specimen RWD_01 shown in Fig. 13. To the right of the red line is the fracture surface created with the roller wedge, while to the left is the fracture surface caused by opening the specimen completely with use of lab tools to be able to inspect the fracture surface of the specimen. This is the same behaviour of the failure surface as observed in the DCB tests.

Table 3 shows an overview of the average results obtained from the specimens tested with the RWD test method, where $F_{push}$ and $\theta_c$ are the average values measured between $d_{ini}$ and $d_{lim}$ and are the test results' output values used in the RWD force and RWD J-integral data reduction methods to determine fracture toughness.

### 3.3. Manual loaded RWD test

The force and energy release rate against the roller wedge displacement curves of the two specimens tested with the RWD test setup loaded by manually driving the roller wedge into the specimen are shown in Fig. 14. The initial stiffness of all three specimens are very similar. After the peak force, the measured force of both specimens converges to 90 N, and the energy release rates to 3 N/mm. The same type of plots, as with the RWD test, are plotted in Fig. 15, the energy release rate against crack extension is plotted (R-curve), and in Fig. 16 the energy release rate calculated with the RWD J-integral method.

Table 4 shows the average values from the crack propagation phase. It can be observed that the average calculated fracture toughness using the RWD force data reduction method is significantly higher compared to the average fracture toughness obtained with the RWD J-integral method.

After the test, the displacement data from the LVDT was used to determine the actual displacement rate applied for the RWD manual test. Fig. 17 shows the slope of the displacement–time plot which equals the displacement rate. For RWD-M_01, this is 41.4 mm/min (0.69 mm/s), for RWD-M_02 and RWD-M_03 this is 36.6 mm/min (0.61 mm/s). A test machine can control a displacement rate very precisely, it is more difficult to do the manual test at a constant and pre-determined displacement rate using a spanner to rotate a threaded bar by hand. As can be seen in Fig. 17, the displacement rate over the whole test appears to be constant, but there are small fluctuations visible in the plotted lines.

### 3.4. Summary of results for ERR of DCB, RWD and RWD manual load

An overview of the average fracture toughness values for the different test methods and data reduction methods is shown in Fig. 18. With a similar standard deviation, the CBT and DCB J-integral methods correlate well for the DCB test. For the RWD test, the RWD force and RWD J-integral data reduction methods do not correlate as well with the benchmark fracture toughness from the DCB test: the RWD force data reduction method is 11% higher and the RWD J-integral method 15% lower compared to the DCB results. For the RWD manual test, the difference increases to 20% for the RWD force data reduction method while the difference remains similar at 14% lower compared to the DCB result for the RWD J-integral method. Looking at the results for both RWD force methods (test machine and manual), there is a 8% increase in measured fracture toughness measured when the RWD manual test is compared to the RWD machine

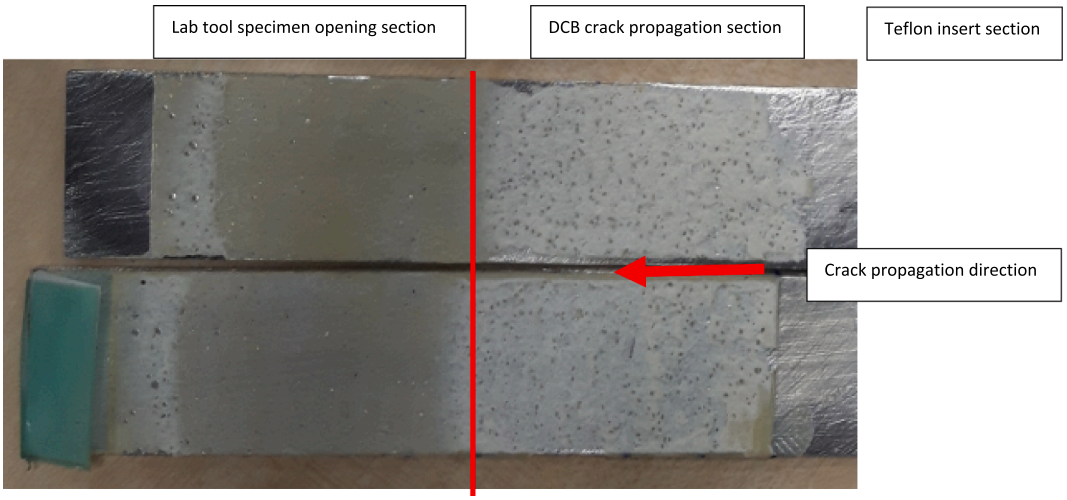


**Fig. 13.** Cohesive fracture surface of specimen RWD_01. To the right of the red line the adhesive is fractured with the roller wedge, while to the left of the red line the specimen was fractured post-test by splitting the adherends completely with lab tools to be able to inspect the fracture surface (later not part of the test).

**Table 3**
Overview of average RWD test results. The standard deviations in the column are the standard deviations found for the result of one specimen. The standard deviation in the last row is the standard deviation found when taking the average value for all specimens tested.

| Specimen | $F_{push}$(N) | | $\theta_c$(°) | | $G_c$– RWD force (N/mm) | | $G_c$– RWD J-int (N/mm) | |
|---|---|---|---|---|---|---|---|---|
| | Avg. | Std. Dev. | Avg. | Std. Dev. | Avg. | Std. Dev. | Avg. | Std. Dev. |
| RWD_01 | 88.81 | 3.76 | 5.50 | 0.07 | 3.020 | 0.122 | 2.161 | 0.114 |
| RWD_02 | 86.66 | 5.15 | 5.64 | 0.04 | 2.945 | 0.167 | 2.413 | 0.070 |
| RWD_03 | 94.56 | 9.60 | 5.59 | 0.13 | 3.201 | 0.310 | 2.574 | 0.229 |
| RWD_04 | 85.06 | 8.58 | 5.43 | 0.11 | 2.896 | 0.278 | 2.138 | 0.177 |
| Average: | 88.77 | | 5.54 | | 3.016 | | 2.322 | |
| Std. Dev. | 3.60 | | 0.08 | | 0.120 | | 0.180 | |

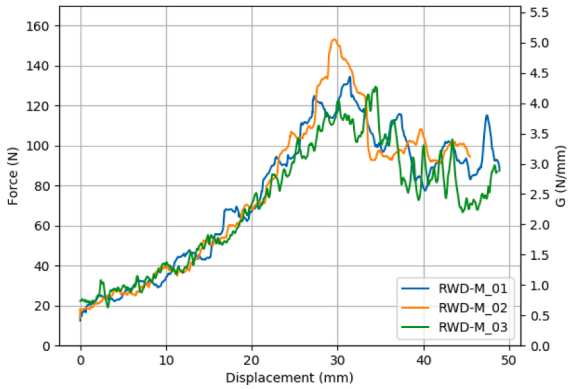


**Fig. 14.** Force and energy release rate vs. wedge displacement curves of manually loaded RWD specimens.

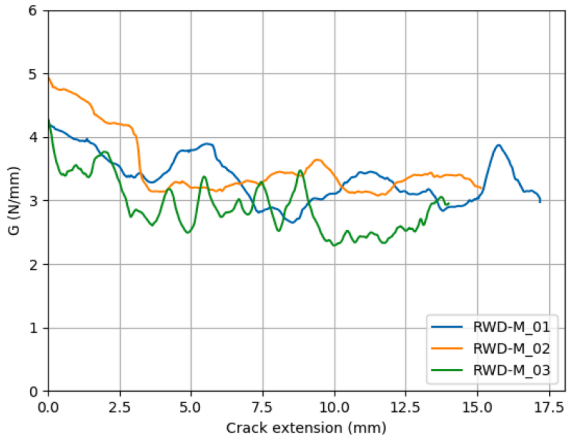


**Fig. 15.** Resistance curves (R-curves) of RWD manually loaded specimens.

test.

## 4. Discussion

In this section, observations from the test results and the RWD methods are discussed. Some parameters concerning sensitivity on the fracture toughness data reduction method are discussed. Finally, the RWD manually loaded test is discussed and compared to the RWD machine loaded test.

### *4.1. Simplified vs exact contact point for the roller wedge*

As mentioned in section 2, the diameter of the roller wedge rollers are assumed to be small enough that the error introduced by using the simplified contact point and RWD force data reduction method does not result in a significant error in the calculation of the

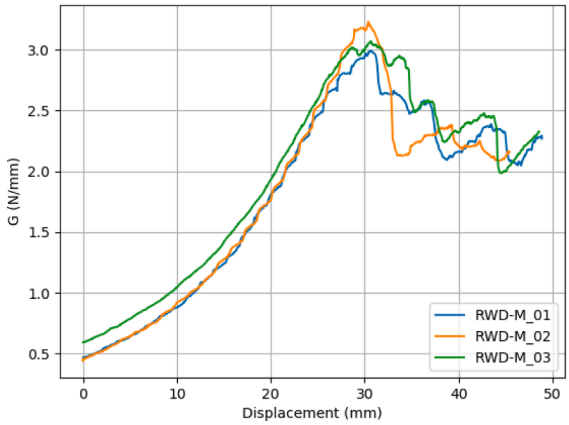


**Fig. 16.** Energy release rate vs. roller wedge displacement of RWD manually loaded specimens determined with the RWD J-integral method.

**Table 4**
Overview of average RWD manually loaded specimen test results. The standard deviations in the column are the standard deviations found for the result of one specimen. The standard deviation in the last row is the standard deviation found when taking the average value for all specimens tested.

| Specimen | $F_{push}$(N) | | $\theta_c$(°) | | $G_c$– RWD force (N/mm) | | $G_c$– RWD J-int (N/mm) | |
|---|---|---|---|---|---|---|---|---|
| | Avg. | Std. Dev. | Avg. | Std. Dev. | Avg. | Std. Dev. | Avg. | Std. Dev. |
| RWD-M_01 | 98.36 | 11.6 | 5.59 | 0.11 | 3.328 | 0.374 | 2.324 | 0.186 |
| RWD-M_02 | 105.58 | 16.02 | 5.57 | 0.18 | 3.550 | 0.511 | 2.360 | 0.323 |
| RWD-M_03 | 84.78 | 11.35 | 5.41 | 0.1 | 2.878 | 0.367 | 2.313 | 0.161 |
| Average: | 96.24 | | 5.523 | | 3.252 | | 2.332 | |
| Std. Dev. | 8.623 | | 0.081 | | 0.280 | | 0.020 | |

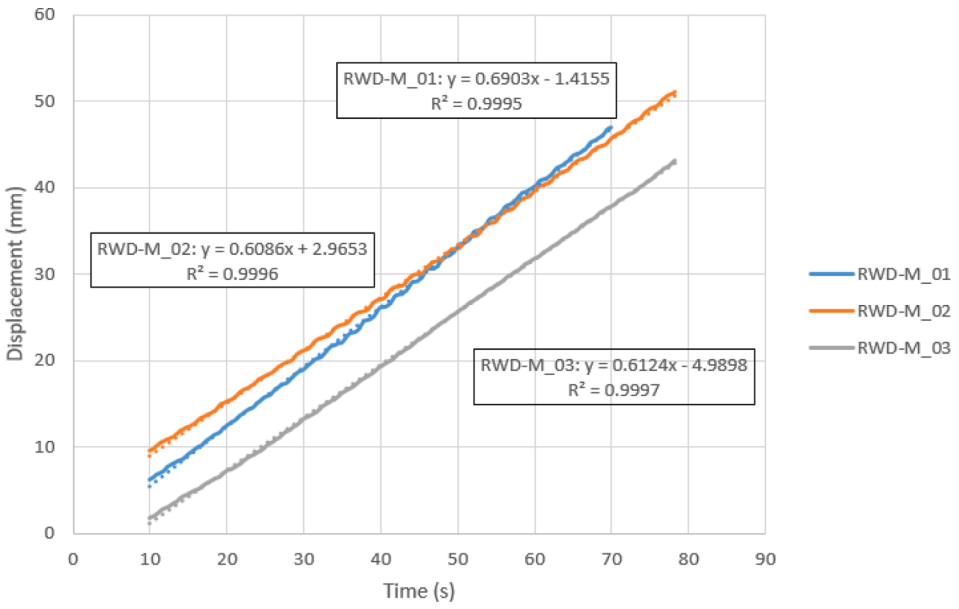


**Fig. 17.** Displacement-time plot of RWD manual test with the slope indicated, which equals the displacement rate.

energy release rate. The graph to the left in Fig. 19 shows there is no visible difference for the determination of the energy release rate using the exact ($G_e$) or simplified contact point ($G$) [6,20], the blue and orange lines are practically on top of each other. This is also visible in the graph to the right in Fig. 19, where the numerically solved crack length for the simplified and exact contact point are shown, $a$ and $a_e$ respectively. During the crack propagation phase the difference is less than 1% and, therefore, the simplified method is used for the RWD test setup. There is a more significant difference between the crack length $a$ and the corrected crack length $a_c$

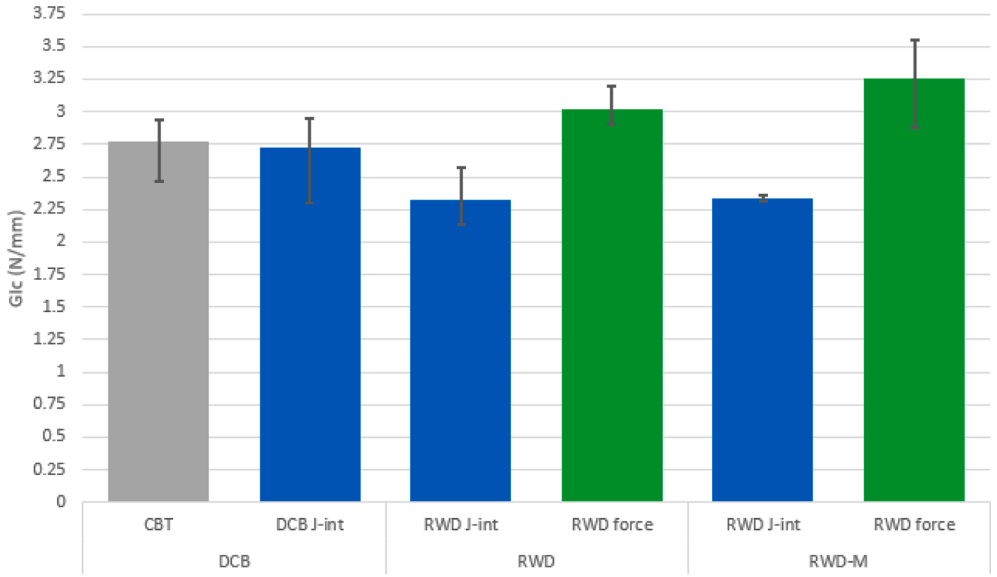


**Fig. 18.** Overview of average fracture toughness (and minimum and maximum values) results for the DCB, RWD and RWD Manual tests when using different data reduction methods (CBT, RWD J-int and RWD force).

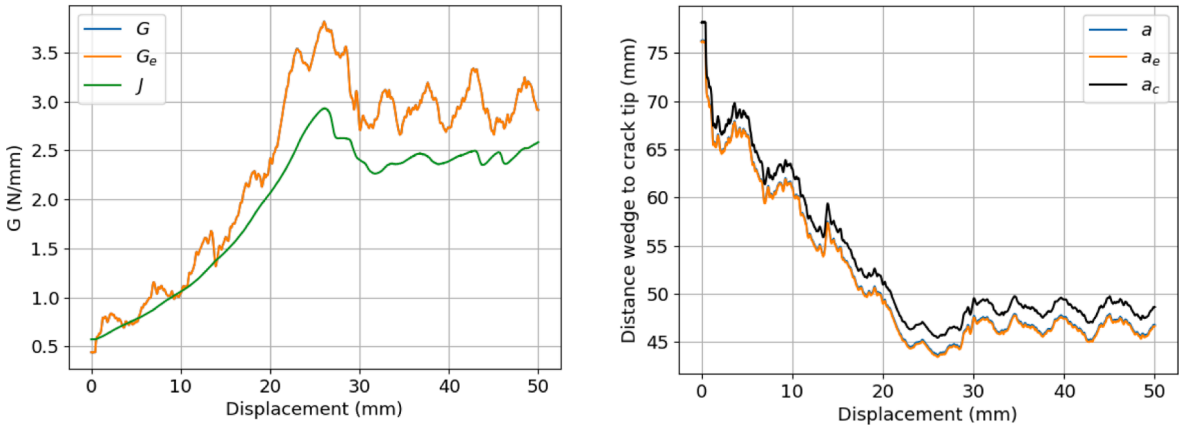


**Fig. 19.** Left: Specimen RWD_02 showing the difference between using the simplified and exact contact point for the RWD force data reduction method. Right: specimen RWD_01 plot of the numerically solved crack length with the simplified contact point $a$, for the exact contact point $a_e$ and the corrected crack length..$a_c$

(equation (3)), therefore, the correction of the crack length cannot be neglected.

### *4.2. Overestimation of the calculated ERR when the RWD data reduction method is used*

During the crack propagation phase there is a significant difference in the energy release rate determined with the RWD force reduction method and the RWD J-integral (Fig. 19 left). The roller wedge rollers have a low rolling resistance and it is assumed that this is much lower compared to, for instance, a sliding wedge which has a typical friction coefficient of about 0.3 (metal on metal) [20]. With the roller wedge, the energy dissipated by the test setup is considered to be low enough to be neglected and therefore the friction coefficient $\mu$ in the data reduction method is taken as zero [21] (as described in section 2.1). However, the energy addressed to the fracture toughness is higher compared to the J-integral, and thus energy has to be dissipated somewhere else in the system. The assumption of zero friction for a roller wedge, as proposed by Glessner et al. [21] seems to overestimate the calculated fracture toughness. One of the most likely locations for energy loss are the roller wedge rollers. It is not easy to determine the energy loss caused by rolling resistance. There could be different factors that influence such resistance, for instance, the type of load, wheel diameter, roller material/hardness, adherend material/finish and/or adherend surface conditions [28]. During the post-processing of the test results with the RWD force data reduction method, a value for the friction coefficient μ of 0.02 was found. Implementing this value makes the results of the energy release rate determined with the RWD force data reduction method correlate better with the RWD J-

integral method, as can be seen in Fig. 20. A friction coefficient of 0.02 is a small value compared to the friction coefficient of a sliding wedge, although it is clear from the results that the energy loss due to the rolling resistance of the rollers cannot be neglected in the RWD force data reduction method.

### 4.3. Sensitivity of the measured rotation angle and force

The RWD J-integral data reduction method presented in section 2.1 (equation (10)) has only the adherend rotation angle $\theta$ as the required measured value from the test. The average measured angle of the RWD specimens is 5.6°with a standard deviation of 0.11. The RWD force data reduction only has the measured force $F_{Push}$ as an input value which is required from the test results. The average measured $F_{Push}$ of the RWD specimens is 89 N with a standard deviation of 3.4. For the RWD J-integral and RWD force data reduction method the spread measured for $\theta$ or $F_{Push}$ is amplified differently when the fracture toughness for a specimen is calculated, due to the behaviour of the data reduction methods, which is linear for the RWD force and exponential for the RWD J-int. The average measured force (89 N) and angle (5.6°) are normalized to 1. The same is done for the fracture toughness obtained with both data reduction methods using the average measured force and angle. This is depicted in Fig. 21, where both data reduction methods are plotted with the normalized average measured test input value ($\theta$ and $F_{Push}$) against the normalized calculated energy release rate. By using equation (6) presented in section 2.1, Fig. 21 is plotted over a range from zero to two times the normalized average force measured for the RWD specimens. Equation (10) from section 2.1 is also plotted in Fig. 21 over a range from zero to two times the normalized average $\theta$ measured for the RWD specimens. With Fig. 21 it is intended to show the difference of both data reduction methods in a qualitative way. The standard deviation is used to show the effect of an error or variation in the measurement on the calculation of the fracture toughness. A range of four times the standard deviation (4*SD) from the average can be applied to check the effect on the calculated fracture toughness [29]. Expressing the 4*SD as a fraction of the average for $\theta$ and $F_{Push}$, this becomes 0.08 and 0.15, respectively, which are shown in Fig. 21 as dotted lines for the $\theta$ and dashed lines for $F_{Push}$. It can be observed that the standard deviation for the $\theta$ is lower than the standard deviation of $F_{Push}$ measured over all the RWD specimens, but that the spread obtained when calculating the fracture toughness higher for the RWD J-integral data reduction method compared to the RWD force data reduction. This means that, compared to the RWD J-integral data reduction method, the RWD force data reduction method is less affected by spread in the test measurement data and, therefore, is a more robust data reduction method. Another factor that increases the possible error in the RWD J-integral is the measurement of the $\theta_{ini}$ as described in section 3.2. The inclinometers are situated at the adherend tips of the non-adhesive side of the specimen, the initial angle of the adherend tips need to be determined for the RWD J-integral data reduction method. It is very difficult to measure the correct thickness of the specimen at the adherend tips when there is no adhesive present. Therefore, it is assumed the adherends are completely straight so the initial angle of $\theta$ can be calculated by measuring the specimen thickness at two points where there is adhesive located. Since the average found $\theta_{ini}$ is small, also a small estimation error on the straightness of adherends has a significant effect on the fracture toughness calculation. Potentially, this could also explain why there is a difference observed in the results of the RWD J-integral and DCB J-integral data reduction method, because the DCB J-integral does not require an initial $\theta$ correction.

### 4.4. Selecting the location of $d_{ini}$

Another factor that influences the calculated fracture toughness of a specimen is where the location of $d_{ini}$ is selected. As described in section 3.2 and shown in Fig. 10, the location of $d_{ini}$ is selected at the infliction point that can be observed in the rotation angle graphs of the inclinometers, which also correlates with the peak force in the force–displacement curve. However, this infliction point is not always very clear, especially when the location of $d_{ini}$ is selected based on the force measurement as required in the RWD force data reduction method. For example, take specimen RWD_02 shown in Fig. 22, in the lefthand plot the $d_{ini}$ is taken at the first infliction point but then the rotation angle increases slightly more, followed by a second infliction point. It can also be observed in the

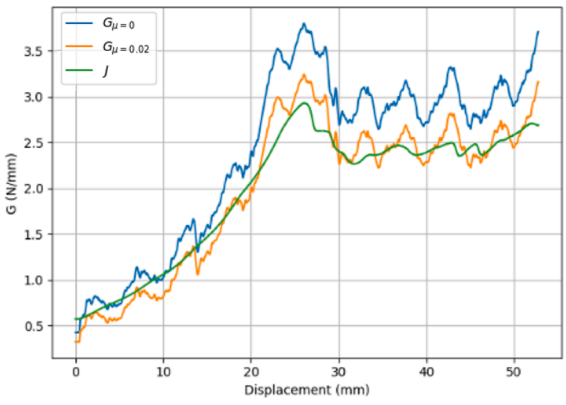


**Fig. 20.** Effect of friction parameter μ on the energy release rate G, results from specimen RWD_01 where the RWD J-integral functions as a reference value.

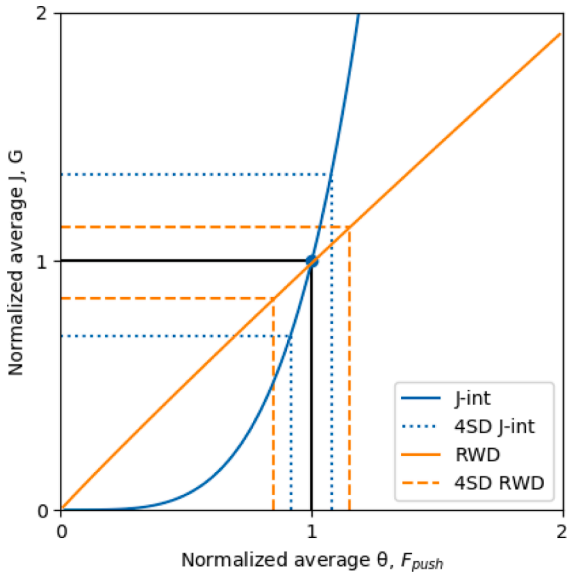


**Fig. 21.** Sensitivity of RWD J-integral data reduction method compared to RWD force data reduction method with the normalized average angle $\theta$ and force $F_{Push}$ plotted against the normalized average calculated J and G.

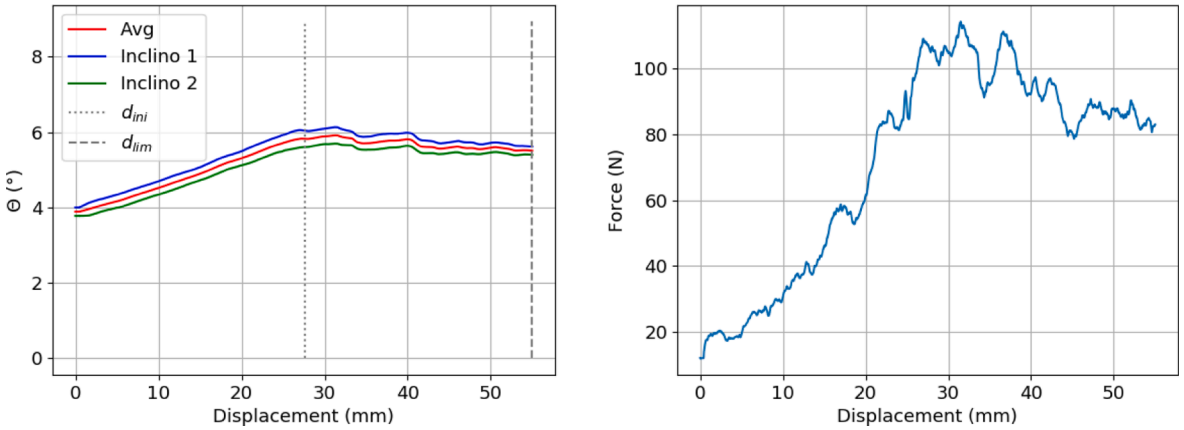


**Fig. 22.** Specimen RWD_03. Left: adherend rotation angle plot with $d_{ini}$ and $d_{lim}$ cut-off displacements indicated with dashed lines. Right: force–displacement plot showing multiple peaks at maximum force before the force declines.

force–displacement curve, Fig. 22 righthand plot, that there are three peaks at a similar force before the force declines to a more stable level later in the test. All the specimens tested show an initial high peak and this is very likely to be material-specific behaviour. However, for the force measurement most specimens show a clearer after-peak phase compared to the example specimen RWD_03.

The difference between the measured peak force and the average force measured later during the more stable phase of the test is more than 10% for most specimens. Therefore, including part of the peak will have an influence on the average calculated fracture toughness of that specific specimen. Consequently, a conservative approach could be taken where the $d_{ini}$ line is selected far enough from the initial peak. However, this could result in a rather short measuring range for the fracture toughness calculation, and due to the fluctuations observed it is desirable to have a long crack propagation phase. Since $d_{lim}$ is limited by the roller wedge encountering the adhesive of the bonded joint, the available measuring range with this specific wedge and specimen combination could be considered a limitation.

### *4.5. RWD test compared with the RWD manual test*

The RWD test setup is a rather simple experimental test device that requires a DCB-like specimen, a wedge driving force and a load cell to measure the wedge driving force during the test. For the tested specimens, the force did not exceed 160 N as can be observed in Fig. 23. This is an amount of force that can be applied by a human hand. A spanner and a threaded bar are used to apply a certain displacement rate to the roller wedge. For all the specimens, once the peak force is reached, the force then tends to drop sharply. This

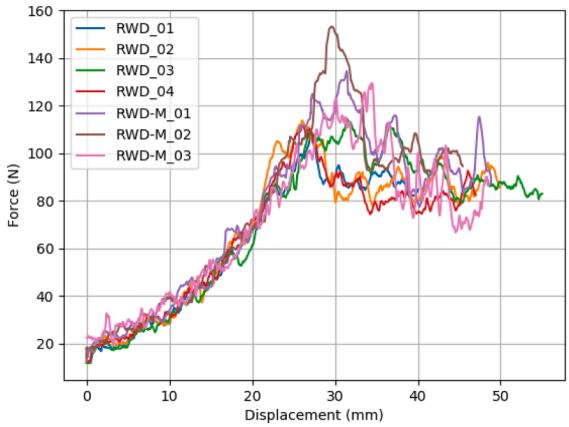


**Fig. 23.** Force-displacement curve comparison between the RWD test (RWD_01 to RWD_04) and RWD manual test (RWD-M_01 to RWD-M_03) specimens.

effect is more significant for the RWD manual test specimens compared to the RWD machine test specimens. Later, during the test, the measured force of both methods is much more similar, as can be seen in the plotted R-curve in Fig. 24. The overview plot of the different test methods in section 3.4 (Fig. 18) clearly shows a difference in the calculated fracture toughness for the RWD manual and RWD machine tests. The difference in calculated fracture toughness between the RWD manual and machine test method is probably caused by the rate sensitivity of the adhesive. The wedge displacement rate of the manual test is eight times higher compared to the machine test. Furthermore, the displacement rate of the manual test appears constant over the whole test, but locally it shows fluctuation, which likely influences the results when a rate dependent adhesive is tested. The higher peak force observed for the manual test, as can been seen in Fig. 23, and the change of fracture surface visible when the specimens are opened with a high rate using lab tools (Fig. 8 & Fig. 13) also indicate rate sensitivity. If a non-rate sensitive adhesive would be tested, it is possible that the RWD test could be performed without a test machine and skilled technicians, but this deserves further investigation by testing more and different materials with the RWD test method.

## 5. Conclusions

This work proposes a relatively small and simple mode I fracture toughness test setup that can potentially be used without a test machine to make quick and affordable approximation of the mode I fracture toughness and qualitatively check the bond quality of the bonded joint, for preliminary design purposes. Using a roller wedge instead of a sliding wedge significantly reduces the wedge resistance. Reducing the resistance of a wedge also reduces the force required to drive the wedge into a specimen. A human hand is capable of applying the low driving force to the roller wedge by turning a thread bar with a spanner. This could be done outside a test machine as long as the adhesive is not rate sensitive, since controlling the wedge displacement is difficult.

At first, the assumption was made that the resistance would be small enough that the friction coefficient can be neglected. However, test results between the RWD force data reduction method and the RWD J-integral method have shown that an amount of energy is dissipated by the system and that it cannot be neglected. It is likely that this energy is dissipated by the resistance of the rollers.

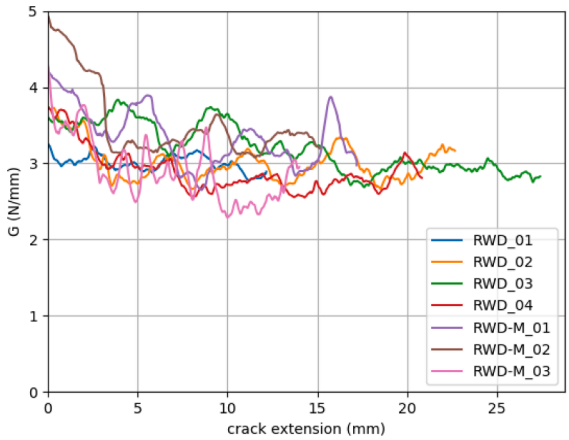


**Fig. 24.** R-curves of the RWD test (RWD_01 to RWD_04) and RWD manual test (RWD-M_01 to RWD-M_03) specimens.

The sensitivity of the measured rotation angle ($\theta$) and force ($F_{Push}$) as input values for respectively the RWD J-integral and RWD force reduction methods are discussed. It is observed that a small spread in the measured rotation angle is amplified in the RWD J-integral method introducing a significant error in the fracture toughness calculation. On the other hand, it has been shown that in the RWD force data reduction method, spread in the measurement is not amplified for the calculation of the fracture toughness, making the RWD force data reduction method more robust than the RWD J-integral data reduction method.

The RWD test setup is relatively simple and small, in theory, if a non-rate sensitive specimen is tested, then the RWD manual test could be performed anywhere as long there is a data acquisition system available to log the force applied to the wedge during the test. However, the difference observed between the RWD machine and manual test is likely related to the rate sensitivity of the adhesive used for this research. For rate sensitive adhesives, a small electrical engine that turns the threaded bar, could be introduced to have a more constant wedge displacement, instead of the need of using a test machine. The RWD test method deserves further investigation by testing different materials and at different displacement rates.

*CRediT authorship contribution statement*

**E. Meulman:** Writing – review & editing, Writing – original draft, Visualization, Validation, Methodology, Investigation, Formal analysis, Data curation, Conceptualization. **J. Renart:** Writing – review & editing, Methodology, Investigation, Conceptualization. **L. Carreras:** Writing – review & editing, Methodology, Investigation, Conceptualization. **J. Zurbitu:** Writing – review & editing, Methodology, Investigation, Conceptualization.

## Declaration of Competing Interest

The authors declare that they have no known competing financial interests or personal relationships that could have appeared to influence the work reported in this paper.

## Acknowledgements

The authors would like to acknowledge the support of the Spanish Government, Ministerio de Economia y Competitividad, with funding from the Redbone project under contract RTI2018-099373-B-I00. The first author would also like to acknowledge the support received from the Universitat de Girona and Banco Santander through the fellowship grant IFUdG2021-AE, co-funded by the AMADE research group (GRCT0064). Open Access funding provided thanks to the CRUE-CSIC agreement with Elsevier. The work in this research has been made possible by patent 300352094, PCT/ES2020/070074 made available by IKERLAN, S.COOP. (IKER018) and the Universitat de Girona.

## References

[1] L. F. M. da Silva, A. Öchsner, and R. D. Adams, Eds., *Handbook of Adhesion Technology*, 2nd ed. Springer International Publishing AG, 2011. doi: 10.1007/978-3-642-01169-6.
[2] Sørensen BF, Jørgensen K, Jacobsen TK, Østergaard RC. DCB-specimen loaded with uneven bending moments. Int J Fract 2006;141(1-2):163–76.
[3] "ASTM D5528 – 13: Standard test method for mode I interlaminar fracture toughness of unidirectional fiber-reinforced polymer matrix composites," vol. 03, no. Reapproved 2007. American Standard of Testing Methods, pp. 1–12, 2014. doi: 10.1520/D5528-13.2.
[4] "ISO 25217:2009 - Adhesives — Determination of the mode 1 adhesive fracture energy of structural adhesive joints using double cantilever beam and tapered double cantilever beam specimens." p. 24, 2009.
[5] da Silva LFM, Dillard DA, Blackman B, Adams RD, editors. Testing Adhesive Joints: Best Practices. KGaA: First. Wiley-VCH Verlag GmbH & Co; 2012.
[6] Manterola J, Renart J, Zurbitu J, Turon A, Urresti I. Mode I fracture characterization of rigid and flexible bonded joints using an advanced Wedge Driven Test. Mech Mater 2020;148(103534):13. https://doi.org/10.1016/j.mechmat.2020.103534.
[7] Fernández MV, de Moura MFSF, da Silva LFM, Marques AT. Composite bonded joints under mode I fatigue loading. Int J Adhes Adhes 2011;31(5):280–5. https://doi.org/10.1016/j.ijadhadh.2010.10.003.
[8] Sarrado C, Turon A, Costa J, Renart J. An experimental analysis of the fracture behavior of composite bonded joints in terms of cohesive laws. Compos Part A Appl Sci Manuf 2016;90:234–42. https://doi.org/10.1016/j.compositesa.2016.07.004.
[9] Kinloch AJ. Durability of structural adhesives. Netherlands: Springer; 1983.
[10] D. O. Adams, K. L. DeVries, and C. Child, "Durability of adhesively bonded joints for aircraft structures," 2012. http://depts.washington.edu/amtas/events/jams_12/papers/paper-adams_adhesive.pdf.
[11] Broughton W. In: Adhesives in Marine Engineering. Elsevier; 2012. p. 99–154.
[12] "ASTM D3762-03(2010) Standard Test Method for Adhesive-Bonded Surface Durability of Aluminum (Wedge Test) (Withdrawn 2019)." ASTM International, p. 5, 2010. [Online]. Available: https://www.astm.org/Standards/D3762.htm.
[13] Cognard J. The mechanics of the wedge test. J Adhes 1986;20(1):1–13. https://doi.org/10.1080/00218468608073236.
[14] Plausinis D, Spelt JK. Designing for time-dependent crack growth in adhesive joints. Int J Adhes Adhes 1995;15(3):143–54. https://doi.org/10.1016/0143-7496(95)91625-G.
[15] Dillard DA, Pohlit DJ, Jacob GC, Starbuck JM, Kapania RK. On the use of a driven wedge test to acquire dynamic fracture energies of bonded beam specimens. J Adhes 2011;87(4):395–423. https://doi.org/10.1080/00218464.2011.562125.
[16] Brown N, Adams D, Devries L. Test method development for environmental durability of bonded composite joints. The University of Utah; 2013. p. 30.
[17] S. LAZCANO UREÑA, G. SANTACRUZ RODRÍGUEZ, J. A. MAYUGO MAJO, J. COSTA BALANZAT, and J. RENART CANALIAS, "Procedimiento y dispositivo de determinación de la tenacidad a la fractura en un ensayo de introducción y avance forzado de una cuña a través de una unión adhesiva," 2460468, 2014.
[18] Kanninen MF, Popelar CH. Advanced Fracture Mechanics. OXFORD UNIVERSITY PRESS; 1985.
[19] R. Mansour, M. Kannan, G. N. Morscher, F. Abdi, C. Godines, and S. Dormohammadi, "The wedge-loaded double cantilever beam test: A friction based method for measuring interlaminar fracutre properties in ceramic matrix composites," in *Advances in High Temperature Ceramic Matrix Composites and Materials for Sustainable Development*, First edit., vol. CCLXIII, M. Singh, T. Ohji, S. Dong, D. Koch, K. Shimamura, B. Clauss, B. Heidenreich, and J. Akedo, Eds. 2017, pp. 273–282. doi: 10.1002/9781119407270.

[20] Renart J, Costa J, Santacruz G, Lazcano S, Gonzalez E. Measuring fracture energy of interfaces under mode I loading with the wedge driven test. Eng Fract Mech 2020;no. 239:15. https://doi.org/10.1016/j.engfracmech.2020.107210.
[21] Glessner AL, Takemori MT, Vallance MA, Gifford SK. Mode I interlaminar fracture toughness of ud cf composites using a novel wedge-driven delamination design. Compos Mater Fatigue Fract 1989;2:181–200. https://doi.org/10.1520/STP10416S.
[22] Adams D, McCartin H, Sievert Z. Development of Environmental Durability Test Methods for Composite Bonded Joints. *JAMS 2018 Technical Review* The Univeristy of Utah 2018:31.
[23] J. Manterola Najera, J. Zurbitu Gonzalez, M. J. Cabello Ulloa, I. Urresti Ugarteburu, J. Renart Canalias, and A. Turon Travesa, "Procedimiento y aparato para la determinación de la tasa de liberacion de energia de una probeta," 300352094, 2020.
[24] Williams JG. End corrections for orthotropic DCB specimens. Compos Sci Technol 1989;35(4):367–76. https://doi.org/10.1016/0266-3538(89)90058-4.
[25] Paris AJ, Paris PC. Instantaneous evaluation of J and C. Int J Fract 1988;38(1):19–21. https://doi.org/10.1007/BF00034281.
[26] Manterola J, Zurbitu J, Renart J, Turon A, Urresti I. Durability study of flexible bonded joints under stress. Polym Test 2020;88:9. https://doi.org/10.1016/j.polymertesting.2020.106570.
[27] Blackman BRK, Kinloch AJ, Paraschi M, Teo WS. Measuring the mode I adhesive fracture energy, GIc, of structural adhesive joints: The results of an international round-robin. Int J Adhes Adhes 2003;23(4):293–305. https://doi.org/10.1016/S0143-7496(03)00047-2.
[28] D. Lippert and J. Spektor, "Rolling Resistance and Industrial Wheels," *Hamilt. Caster*, no. 888, p. 8, 2013, [Online]. Available: http://www.mhi.org/media/members/14220/130101690137732025.pdf.
[29] Hamby DM. A Review of Techniques for Parameter Sensitivity. Environ Monit Assess 1994;32:135–54. https://doi.org/10.1007/BF00547132.